Title

MiRP2 Forms Potassium Channels in Skeletal Muscle with Kv3.4 and Is Associated with Periodic Paralysis

Authors

Abbott, Geoffrey W
Butler, Margaret H
Bendahhou, Saïd
et al.

Peer reviewed

MiRP2 Forms Potassium Channels in Skeletal Muscle with Kv3.4 and Is Associated with Periodic Paralysis

Geoffrey W. Abbott,* Margaret H. Butler,*
Saïd Bendahhou,† Marinos C. Dalakas,‡
Louis J. Ptacek,† and Steve A. N. Goldstein*§
*Departments of Pediatrics and Cellular
  and Molecular Physiology
Boyer Center for Molecular Medicine
Yale University School of Medicine
New Haven, Connecticut 06536
†University of Utah
Howard Hughes Medical Institute
Salt Lake City, Utah 84112
‡National Institute of Neurologic Diseases and Stroke
National Institutes of Health
Bethesda, Maryland 20892

Summary

The subthreshold, voltage-gated potassium channel of skeletal muscle is shown to contain MinK-related peptide 2 (MiRP2) and the pore-forming subunit Kv3.4. MiRP2-Kv3.4 channels differ from Kv3.4 channels in unitary conductance, voltage-dependent activation, recovery from inactivation, steady-state open probability, and block by a peptide toxin. Thus, MiRP2-Kv3.4 channels set resting membrane potential (RMP) and do not produce afterhyperpolarization or cumulative inactivation to limit action potential frequency. A missense mutation is identified in the gene for MiRP2 (*KCNE3*) in two families with periodic paralysis and found to segregate with the disease. Mutant MiRP2-Kv3.4 complexes exhibit reduced current density and diminished capacity to set RMP. Thus, MiRP2 operates with a classical potassium channel subunit to govern skeletal muscle function and pathophysiology.

Introduction

The *KCNE* genes encode small, single transmembrane-domain peptides that associate with pore-forming potassium channel subunits to form mixed complexes with unique characteristics (Abbott and Goldstein, 1998). The peptides do not function alone. *KCNE1* and *2* peptides are abundant in the heart where they contribute to repolarizing channels that are required for normal cardiac electrical function. Thus, MinK (encoded by *KCNE1*) assembles with KCNQ1 to form IKs channels (Barhanin et al., 1996; Sanguinetti et al., 1996), MiRP1 (MinK-related peptide 1 from *KCNE2*) combines with HERG to form IKr channels (Abbott et al., 1999), and mutations of *KCNE1* (Splawski et al., 1997; Sesti and Goldstein, 1998) and *KCNE2* (Abbott et al., 1999; Sesti et al., 2000) are associated with life-threatening cardiac arrhythmia. Five *KCNE* genes are now known: *KCNE1* (Takumi et al., 1988), *2, 3, 4* (Abbott et al., 1999), and *5* (Piccini et al., 1999).

§To whom correspondence should be addressed (e-mail: steve. goldstein@yale.edu).

Here, the function and disease association of the *KCNE3*-encoded peptide MiRP2 is demonstrated.

Because *KCNE3* transcripts are expressed abundantly in human skeletal muscle, we sought to evaluate a well-recognized but unexplained discrepancy: despite the presence of three channel subunits that form depolarization-activated, rapidly inactivating (A-type) potassium channels when the clones are studied in experimental cells, no such currents are observed in mammalian skeletal muscle cells (Adrian et al., 1970; Beam and Donaldson, 1983). While Kv1.4 and Kv4.1 might have eluded detection because the first is expressed only at low levels and the latter only early in development, Kv3.4 transcript and protein are expressed predominantly and robustly in skeletal muscle throughout life (Lesage et al., 1992; Rettig et al., 1992; Weiser et al., 1994; Veh et al., 1995; Vullhorst et al., 1998). More puzzling, cloned Kv3.4 channels are also characterized by activation at suprathreshold potentials, slow recovery from rapid inactivation, and slow recovery from inactivation (producing afterhyperpolarization, AHP) (Ruppersberg et al., 1991a), and these attributes are not manifest in muscle recordings (Vazquez, 1988; Schroter et al., 1991; Rizzo and Nonner, 1992; Camacho et al., 1996). These findings argue that Kv3.4 displays different attributes in experimental and native cells, perhaps due to the influence of an unrecognized channel subunit. Indeed, a role for a small protein is suggested by the observation that small messenger RNAs from brain can alter A-type channel gating (Rudy et al., 1988; Chabala et al., 1993). For these reasons, we tested the hypothesis that MiRP2 was necessary to generate native skeletal muscle currents with Kv1.4, Kv4.1, or Kv3.4.

We demonstrate here that MiRP2 has no apparent effect on Kv1.4 or Kv4.1, but forms stable complexes with Kv3.4 subunits to alter their single-channel conductance, open probability, and sensitivity to a peptide toxin. Moreover, MiRP2-Kv3.4 channels are demonstrated to have the same attributes as native channels studied in the plasma membranes of C2C12 skeletal muscle cells (where MiRP2 and Kv3.4 are shown to localize). Compared to Kv3.4, native MiRP2-Kv3.4 channels pass more potassium ions due to their larger unitary conductance, faster recovery from inactivation, and slower cumulative inactivation. Because MiRP2-Kv3.4 channels are 80-fold more active at -40 mV, they establish the resting membrane potential (RMP) of C2C12 muscle cells. Due to their rapid recovery from inactivation, MiRP2-Kv3.4 channels do not show AHP-associated reopenings during post-stimulus recovery as do cloned Kv3.4 channels.

Based on these observations (and prior association of *KCNE1* and *2* with cardiac arrhythmia), we hypothesized that mutations in *KCNE3* might be associated with inherited disorders of skeletal muscle. Screening has identified two families in which a missense point mutation encoding R83H-MiRP2 segregates with symptoms and electromyographic abnormalities of periodic paralysis. The mutant MiRP2 is found to form complexes with

Kv3.4 that are abnormal in function, passing less outward current upon activation and demonstrating a diminished capacity to set resting potential compared to wild type. Supporting a direct role in muscle dysfunction, the mutant suppresses wild-type MiRP2-Kv3.4 channel currents in experimental cells and shifts resting potential to abnormally depolarized voltages when it is expressed in skeletal muscle cells. This report explains differences between cloned Kv3.4 channels and native muscle currents, establishes a requirement for wild-type MiRP2 in normal skeletal muscle function, and expands the recognized roles of the *KCNE*-encoded MinK-related subunits by demonstrating that they are not limited to channels formed with *KCNQ* and *HERG* class subunits, but assemble with classical voltage-gated potassium (Kv) channel subunits to determine their behavior as well.

Results

KCNE3 Is Located on Chromosome 11q, Expressed in Skeletal Muscle, and Predicts a 103 Residue Peptide

With a search strategy based on residues critical for *KCNE1* (MinK) function in cardiac I_{Ks} channels, we previously cloned *KCNE2*, *3*, and *4* (encoding MiRP1, 2 and 3) and localized human *KCNE1* and *2* to chromosome 21q22.1 (Abbott and Goldstein, 1998; Abbott et al., 1999). *KCNE5* (encoding MiRP4) was identified by others on a segment of the X chromosome deleted in AMME syndrome (Piccini et al., 1999).

Here, we first localized *KCNE3* to 11q13–14 by radiation hybrid mapping. Thereafter, human tissues were assessed by Northern blotting using a 1 kb fragment of human *KCNE3*, revealing an abundant single message only in skeletal muscle among 16 tissues tested (Figure 1A; day 1); after extended exposure, transcripts were also apparent in samples from heart and brain (not shown, day 10). The same expression pattern was obtained using a 133 bp fragment from the 3′UTR of *KCNE3* as a probe (Experimental Procedures). Multiple identical clones of *KCNE3* were then isolated from human skeletal muscle, heart, and brain as previously described (Abbott et al., 1999). A predicted open reading frame of 309 bp forecasts a peptide of 103 residues with three N-linked glycosylation sites, a single transmembrane (TM) domain, and one consensus sequence for protein kinase C-mediated phosphorylation. Alignment of human MiRP2 and MinK (which has 129 residues) using ClustalW1.6, as before (Abbott et al., 1999), yields two gaps, 22% identity and 39% homology. These attributes suggest that MiRP2 has a Type I membrane topology (external N terminus, a single TM domain, and an internal C terminus) like other *KCNE* subunits (Abbott and Goldstein, 1998) (Figure 1B); in contrast, a 6 TM topology is typical for pore-forming α subunits of voltage-gated potassium channels like Kv3.4 (Figure 1B).

MiRP2 and Kv3.4 Subunits Localize in Skeletal Muscle Plasma Membranes and Form Stable Complexes

Western blot analysis was used to study MiRP2 and Kv3.4 subunits expressed heterologously in Chinese hamster ovary (CHO) cells and to evaluate native expression of the subunits in adult rat skeletal muscle tissue and a murine skeletal muscle cell line (C2C12). Expression of MiRP2 in CHO cells allowed detection of four bands with apparent molecular masses between 14 and 21 kDa after SDS-PAGE separation and visualization with polyclonal rabbit anti-MiRP2 antibodies (Figure 1C, lane 2). As expected for a peptide with three N-linked glycosylation sites, treatment with endoglycosidase F collapsed the four bands to one at the predicted mass of MiRP2 bearing no complex carbohydrate (~14 kDa, Figure 1C, lane 3). The bands were not detected in untransfected cells (Figure 1C, lane 1) or in cells expressing MiRP2 but probed with preimmune serum (not shown). Adult rat sartorius muscle tissue showed the same specific bands for MiRP2, with immature forms becoming visible after overexposure (Figure 1D, lanes 1 and 2). Analysis of C2C12 muscle cells also revealed MiRP2-specific bands between 14 and 21 kDa, with the fully glycosylated form most abundant (Figure 1E, lane 1); again, endoglycosidase F collapsed the bands to a single species at ~14 kDa (not shown).

Expression of Kv3.4 in CHO cells and study of rat sartorius muscle allowed detection of specific bands at ~66 and 97 kDa with commercial anti-Kv3.4 antibodies (Figure 1C, lane 5 and Figure 1D, lane 4). The presence of Kv3.4 protein in C2C12 muscle cells was confirmed by detection of a specific 66 kDa band (Figure 1E, lane 3).

Immunofluorescent staining revealed that native MiRP2 and Kv3.4 subunits were both present in the plasma membranes of C2C12 muscle cells. Thus, MiRP2 and Kv3.4 antibodies demonstrated specific punctate plasma membrane accumulations (Figure 1F, panels 1 and 3, respectively). Moreover, MiRP2 and Kv3.4 subunits formed detergent-stable complexes when coexpressed in the mammalian cell line COS. Thus, specific MiRP2 bands were detected between 14 and 21 kDa in whole cell lysates (Figure 1G, lane 1) and after immunoprecipitation with anti-Kv3.4 (Figure 1G, lane 3).

MiRP2-Kv3.4 Complexes Show Altered Voltage-Dependent Activation and Single-Channel Current

MiRP2 had no significant effect on either Kv1.4 or Kv4.1 (Experimental Procedures). Conversely, Kv3.4 and MiRP2-Kv3.4 channels displayed marked differences in voltage-dependent activation that were apparent in both macroscopic and single-channel current recordings (Figures 2A and 2D). While Kv3.4 channels passed only outward currents when expressed in CHO cells and studied in large cell-attached patches with roughly equal potassium levels on either side of the membrane, MiRP2-Kv3.4 channels passed both inward and outward currents (Figures 2A and 2B). This can be understood from the normalized conductance-voltage relationships for the two channel types (Figure 2C): channels with MiRP2 achieved half-maximal activation at -43.8 ± 1.4 mV while homomeric Kv3.4 channels required significantly greater depolarization ($V_{1/2} = +3.3 \pm 1.9$ mV). This difference was also apparent at the single-channel level where MiRP2-Kv3.4 but not Kv3.4 channels exhibited significant numbers of openings with voltage steps to hyperpolarized potentials (Figure 2D).
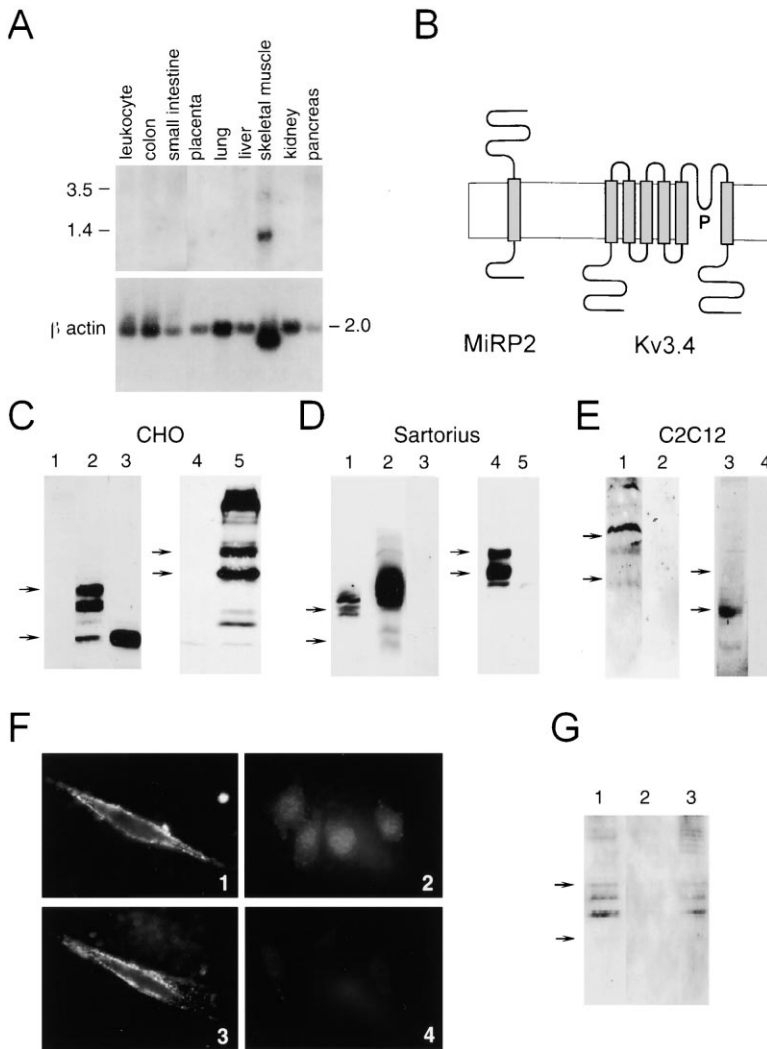
Figure 1. MiRP2 and Kv3.4 Subunits Localize to Skeletal Muscle Plasma Membrane and Form Stable Complexes

(A) Tissue distribution of human *KCNE3* encoding MiRP2. Northern blot of indicated human tissues performed with a 1 kb *KCNE3* fragment (upper panel) and a β-actin probe (lower panel).

(B) Predicted topology of MiRP2 and Kv3.4 channel subunits; P, pore loop domain.

(C) Western blot analysis of CHO cell lysates probed with anti-MiRP2 (lanes 1–3) or anti-Kv3.4 antibodies (lanes 4 and 5). Cells were treated with plasmids containing the genes for: lane 1: untransfected; lane 2: MiRP2; lane 3: MiRP2 (sample treated with endoglycosidase F); lane 4: untransfected; lane 5: Kv3.4. Arrows correspond to apparent molecular weights: lanes 1–3: upper, 21 kDa; lower, 14.5 kDa; lanes 4, 5: upper, 97 kDa; lower, 66 kDa.

(D) Western blot analysis of rat sartorius muscle. Lane 1: probed with anti-MiRP2; lane 2: probed with anti-MiRP2, extended exposure; lane 3: probed with preimmune serum (negative control); lane 4: probed with anti-Kv3.4; lane 5: probed with anti-Kv3.4 after pretreatment with Kv3.4 peptide (negative control). Arrows correspond to apparent molecular weights: lanes 1–3: upper, 21 kDa; lower, 14.5 kDa; lanes 4 and 5: upper, 97 kDa; lower, 66 kDa.

(E) Western blot analysis of C2C12 muscle cell lysates. Lane 1: probed with anti-MiRP2; lane 2: probed with preimmune serum (negative control); lane 3: probed with anti-Kv3.4; lane 4: probed with anti-Kv3.4 after pretreatment with Kv3.4 peptide (negative control). Arrows correspond to apparent molecular weights: lanes 1 and 2: upper, 21 kDa; lower, 14.5 kDa; lanes 3, 4: upper, 97 kDa; lower, 66 kDa.

(F) Surface immunostaining of C2C12 muscle cells. Panels indicate C2C12 cells incubated with (1) anti-MiRP2 antibody; (2) preimmune serum; (3) anti-Kv3.4 antibody; (4) without primary antibody.

(G) Coimmunoprecipitation. Lanes contain lysates of COS cells expressing both HA-tagged MiRP2 and Kv3.4 subunits and were probed with anti-HA antibody; (1) total lysate; (2) after IP with control antiserum; (3) after IP with anti-Kv3.4. Arrows: upper, 21 kDa; lower, 14.5 kDa.

Another effect of MiRP2 was to increase the amplitude of single-channel currents. Thus, Kv3.4 channels had smaller unitary currents than MiRP2-Kv3.4 complexes due primarily to voltage-dependent current rectification (Figures 2E and 2F). The slope conductance from 10–50 mV was 21 ± 0.9 pS for Kv3.4 channels while it was 26 ± 0.5 pS for MiRP2-Kv3.4 complexes; (unitary currents at +60 mV were 1.6 ± 0.1 and 2.0 ± 0.1 pA for Kv3.4 and MiRP2-Kv3.4 channels, respectively).

C2C12 Skeletal Muscle Cells Express a Native Channel with Biophysical and Pharmacological Characteristics of MiRP2-Kv3.4 Complexes

As C2C12 muscle cells display both MiRP2 and Kv3.4 on their surface (Figure 1F), cell-attached patch recordings were performed (Figure 3). These studies revealed a native potassium channel like MiRP2-Kv3.4 and dissimilar to Kv3.4 in ~20% of patches (n ~250 cell-attached patches studied). To quantify the attributes of this native channel, patches were discarded (~50%) if they contained any other channels (Experimental Procedures). The native channel was like MiRP2-Kv3.4 channels in CHO cells in that it passed potassium (Figure 3A), was opened by depolarization with a subthreshold midpoint activation voltage (Figures 3A and 3B), was inactivating (Figure 3B), and had the same unitary current amplitude and rectification behavior (Figure 3C), similar steady-state open probability (Figure 4A), similar open state dwell times (Figure 4B), and identical sensitivity to a peptide toxin (Figure 5).

Thus, both channels passed potassium and were activated by steps to negative voltages where Kv3.4 channels are silent (Figures 2D and 3A). The native channel displayed a single-channel current amplitude of 2.1 ± 0.1 pA at +60 mV and a slope conductance of 31 ± 0.4 pS between +10 and +50 mV (Figures 3A and 3C) similar to values observed for MiRP2-Kv3.4 complexes (but not Kv3.4 channels) in CHO cells (Figures 2D–2F). When single native channels were stepped repetitively from −80 to +60 mV, they activated rapidly with an apparent
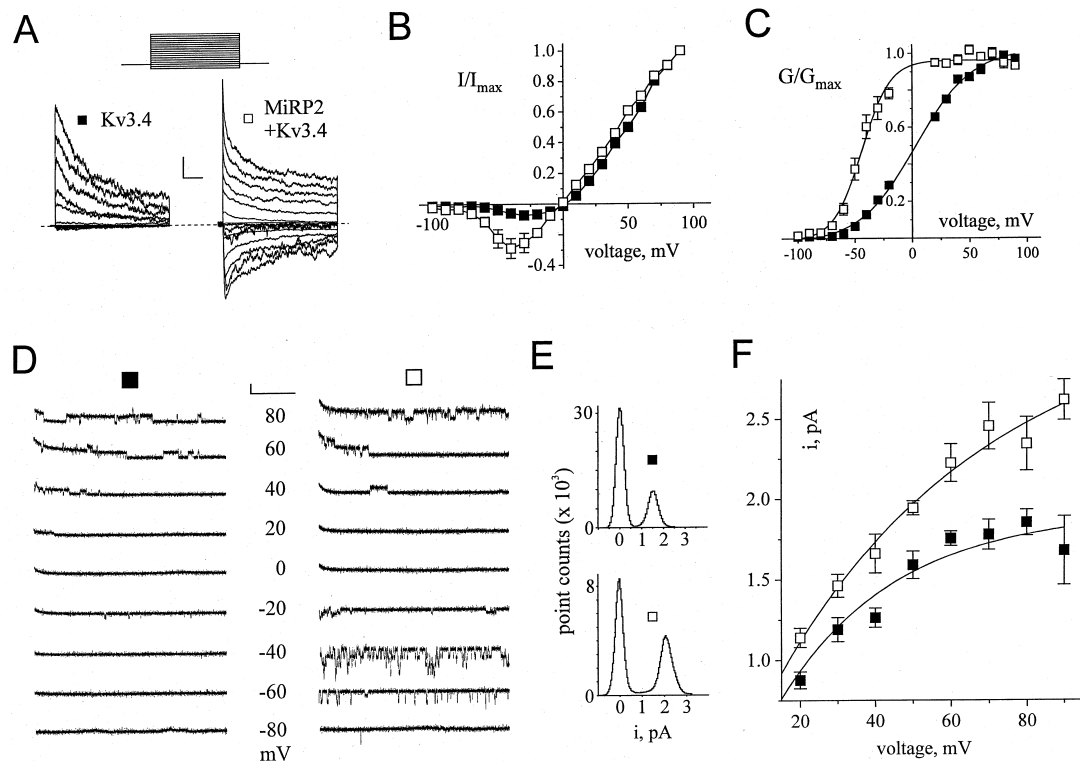
Figure 2. MiRP2-Kv3.4 Channels Activate More Readily and Have a Larger Unitary Conductance than Kv3.4 Channels

Studies of Kv3.4 channels (solid squares) and hMiRP2-Kv3.4 complexes (open squares) were performed in CHO cells in on-cell patch configuration with 100 mM KCl solution in bath and pipette using Protocol 1 (A–D) and Protocol 2 (E and F) (Experimental Procedures). Data were collected at 5 kHz, digitally filtered at 1 kHz or 500 Hz. Error bars represent SEM.

(A) Representative current families between −100 and 60 mV in patches with high channel density (inset, Protocol 1); scale bars 50 pA and 500 ms, dashed line represents zero current level.

(B) Normalized peak current voltage relationship for recordings as in (A) (n = 16–19 patches).

(C) Normalized conductance-voltage relationship for patches in (B). Curves were fit to a Boltzmann function: $1/\{1 + \exp[(V_{1/2}-V)/V_s]\}$, where $V_{1/2}$ is the half-maximal voltage of activation and V_s the slope factor. Kv3.4 channels showed: $V_{1/2} = 3.3 \pm 1.9$ mV, $V_s = 24.5 \pm 1.6$ mV; MiRP2-Kv3.4 channels showed: $V_{1/2} = -43.8 \pm 1.4$ mV, $V_s = 12.4 \pm 1.3$ mV.

(D) Representative current families between −80 mV and 80 mV in patches containing ∼5 channels, scale bars 2 pA and 1 s.

(E) Representative all-points histograms computed at 60 mV; does not reflect open probability.

(F) Current-voltage relationships for single Kv3.4 or MiRP2-Kv3.4 channels in cell-attached patches (n = 4–6) studied at the indicated voltages. All-points histograms constructed with $>2 \times 10^5$ events (>500 transitions) per voltage per patch.

mean first latency of ∼45 ms (Figure 3B). Fifty consecutive pulses showed ten null records and an ensemble with kinetics like those of MiRP2-Kv3.4 complexes in CHO cells (Figures 2A and 3B).

While cloned Kv3.4 channels were not activated at potentials negative to −20 mV, as expected (Schroter et al., 1991), MiRP2-Kv3.4 complexes in CHO cells and native channels in C2C12 cells showed both activation and a significant steady-state open probability (P_o) at hyperpolarized potentials. This was quantified for single channels in on-cell patches held at −40 mV for 5–10 min (Figure 4). Whereas Kv3.4 channels opened rarely and briefly, MiRP2-Kv3.4 and native channels opened frequently and for longer duration (Figure 4A). All-points histograms reported a P_o of 0.0005 ± 0.0003 for Kv3.4 channels whereas MiRP2-Kv3.4 and native channels were open 80- to 100-fold more often with P_o values of 0.04 ± 0.01 and 0.05 ± 0.02, respectively (Figure 4B, upper panels, n = 4–5 patches). While Kv3.4 channel openings were short-lived with dwell times that were best fit to a single exponential ($\tau = 2.6 \pm 0.06$ ms), both MiRP2-Kv3.4 and native channel open times were best

fit by a sum of two exponential terms with time constants of 1.80 ± 0.03 and 21.0 ± 0.1 ms and 1.6 ± 0.2 and 15.5 ± 0.1 ms, respectively (Figure 4B, lower panels, n = 4–5 patches).

MiRP2-Kv3.4 and native channels also showed similar inhibition by the peptide toxin blood-depressing substance 2 (BDS-II) (Figure 5). This naturally occurring peptide from the sea anemone *Anemonia sulcata* blocks cloned Kv3.4 channels in the nanomolar range but has negligible effects on other channels in the Kv and Kir families that were tested (Diochot et al., 1998). To study steady-state blockade, BDS-II was applied to the external face of single channels in outside-out patches held at −40 mV. Current inhibition was found to be reversible (not shown) and was observed as a reduction in single-channel open probability for Kv3.4, MiRP2-Kv3.4, and native channels (Figure 5A). Dose inhibition relationships for the three channels were constructed using all-points histograms to quantify relative open probability at various toxin concentrations (Figures 5B and 5C). While Kv3.4 channels demonstrated a half-blocking concentration (K_i) of 0.26 ± 0.06 μM (n = 4 patches), MiRP2-
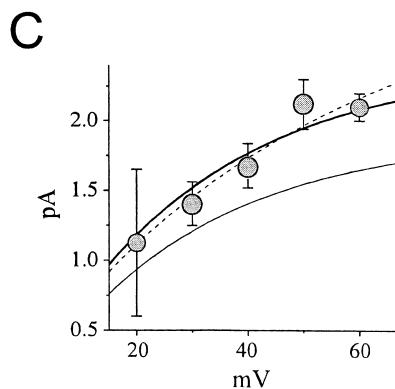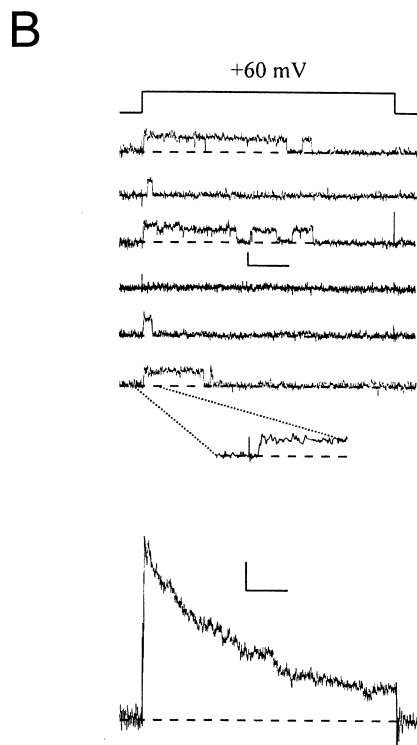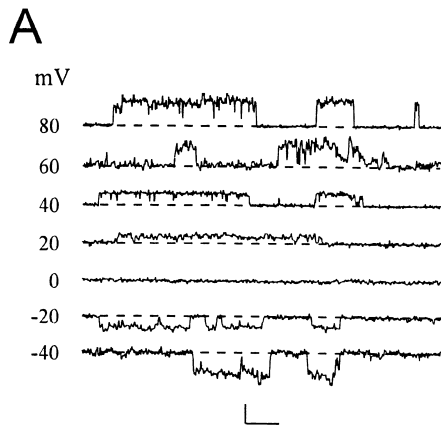
A

B

C

Figure 3. Native MiRP2-Kv3.4-Like Channels Are Observed in a Skeletal Muscle Cell Line

Studies of native channels were performed with C2C12 cells in on-

Kv3.4 and native channels in C2C12 cells were $\sim$30-fold less sensitive with K_i values of 7.2 $\pm$ 1.8 and of 6.9 $\pm$ 2.7 μM, respectively (n = 3–4 patches).

MiRP2-Kv3.4-Like Channels in C2C12 Muscle Cells Set Resting Membrane Potential (RMP)

Their activity at negative potentials suggested that MiRP2-Kv3.4 and native channels should influence resting membrane potential while Kv3.4 channels might not. To test this hypothesis, whole-cell current clamp was performed with a nystatin-perforated patch technique with physiological levels of bath potassium (4 mM) (Figure 6). CHO cells expressing Kv3.4 had a mean resting membrane potential (RMP) of −44 $\pm$ 3 mV (n = 11) similar to that for mock-transfected cells (not shown). Conversely, CHO cells expressing MiRP2-Kv3.4 channels had a RMP of −61 $\pm$ 4 mV (n = 8). To determine the contribution of the channels to resting potential, BDS-II was added at a level sufficient to completely inhibit both Kv3.4 or MiRP2-Kv3.4 channels (30 μM). Application of BDS-II to cells expressing Kv3.4 channels did not significantly shift RMP (−43 $\pm$ 4 mV, n = 7) supporting the idea that these channels did not influence resting potential. In contrast, toxin applied to CHO cells expressing MiRP2-Kv3.4 channels produced a shift of $\sim$20 mV in RMP to −43 $\pm$ 1 mV (n = 5). Native MiRP2-Kv3.4-like channels in C2C12 cells were found to exert similar control over resting potential. Thus, C2C12 cells had an RMP of −65 $\pm$ 4 mV (n = 9) under control conditions and showed a shift of $\sim$20 mV to −46 $\pm$ 2 mV (n = 4) with application of 30 μM BDS-II.

MiRP2-Kv3.4 channels influence RMP not only because they activate at hyperpolarized potentials (Figure 2C), but because they continue to pass outward potassium current at steady state; this is apparent at both the single-channel (Figure 4B) and macroscopic levels (Figure 6B). Thus, the macroscopic Kv3.4 "window" conductance (derived from steady-state, voltage-dependent inactivation and activation relationships) had a peak above 0 mV and was small below threshold (Figure 6C, upper) while the "window" for MiRP2-Kv3.4 was maximal at −40 mV and of significant magnitude at subthreshold potentials (Figure 6C, lower).

### MiRP2 Alters Rate of Recovery from Inactivation and Cumulative Inactivation

Cloned Kv3.4 channels show "fast" or A-type inactivation with maintained depolarization due to occlusion of

---

cell patch mode with 100 mM KCl in bath and pipette. Data were collected at 5 kHz, digitally filtered at 1 kHz or 500 Hz.
(A) Representative openings between −40 mV and 80 mV in a patch with $\sim$5 channels by Protocol 1; scale bars 2 pA and 100 ms.
(B) Voltage activation of single native C2C12 channels. (Top Panel) Six representative traces during repetitive pulsing to 60 mV from a holding voltage of −80 mV (inset, voltage Protocol 2); expanded record for a trace with an apparent first latency of $\sim$40 ms (Experimental Procedures). (Bottom panel) Ensemble average of 50 consecutive pulses to 60 mV. Scale bars 2 pA (top panel), 0.5 pA (bottom panel), and 500 ms.
(C) Current-voltage relationships for single native C2C12 channels in cell-attached patches (n = 3–6) at the indicated voltages (Protocol 1). Error bars are SEM. All-points histograms constructed with >5 $\times$ 10^3 events (>10 transitions) per voltage per patch. C2C12 channels (circles, thick line); Kv3.4 channels in CHO cells (thin line); MiRP2-Kv3.4 channels in CHO cells (dashed line).
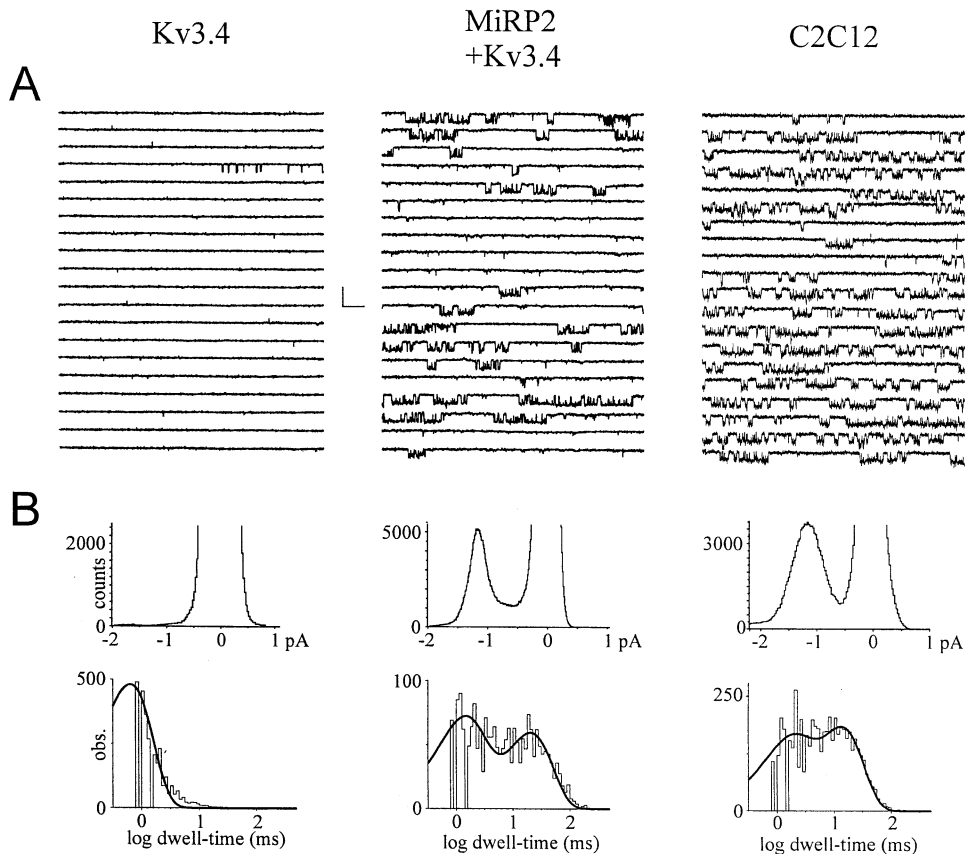
Figure 4. MiRP2-Kv3.4 and Native C2C12 Channels Have a Higher Steady-State P_o than Kv3.4 Channels at Negative Potentials

Studies of single Kv3.4 or MiRP2-Kv3.4 channels expressed in CHO cells and native C2C12 cell channels were performed in cell-attached patches at −40 mV (Protocol 3) with 100 mM KCl solution in the bath and pipette. Low-pass filtered at 500 Hz.

(A) Representative steady-state currents in patches containing one channel (cloned channels) or three channels (native C2C12 channels); scale bars 2 pA and 500 ms. The displayed traces are 1 min continuous stretches of 5–10 min recordings at 6 s per line.

(B) (Upper panels) Representative all-points histograms computed from steady-state single-channel patches held at −40 mV for 5–10 min and indicative of P_o (cloned channels) or a three-channel patch indicative of nP_o (native C2C12 channels). Left, Kv3.4 channels; central, MiRP2-Kv3.4 channels; right, native C2C12 channels. (Lower panels) Representative dwell-time histograms computed at −40 mV from patches held at steady state for 5–10 min. Left, Kv3.4 channels; central, MiRP2-Kv3.4 channels; right, native C2C12 channels. Dwell times were fit using the Marquardt Least-Squares method (PSTAT). Kv3.4 channel dwell times were best fit with a single exponential, MiRP2-Kv3.4 and native C2C12 channel with a double exponential function as indicated by thick lines; τ values in text.

the internal pore by N-terminal "ball" residues (Ruppersberg et al., 1991b; Antz et al., 1997). Kv3.4 inactivation rates vary widely with expression environment due to kinase-mediated regulation (Covarrubias et al., 1994; Diochot et al., 1998); conversely, recovery from inactivation is rapid in native cells (50–200 ms) (Rizzo and Nonner, 1992) but slow in experimental expression systems (0.5–1 s) (Ruppersberg et al., 1991a). When inactivation is significant and recovery slow, reopening of channels upon repolarization produces afterhyperpolarization (Ruppersberg et al., 1991b). It appears that MiRP2 underlies the rapidity of recovery from inactivation of native channels and, thereby, suppression of afterhyperpolarization.

Recovery from inactivation was quantified first with whole-cell currents using 3 s depolarizing pulses and progressively longer recovery periods; the time course was best fit with a double exponential function (Figure 7A). MiRP2-Kv3.4 complexes in CHO cells were found to recover by 50% in ~100 ms, at least 5-fold more

rapidly than Kv3.4 channels (Figure 7B). At the single-channel level (in small cell-attached patches), Kv3.4 channels recovered slowly from inactivation showing reopenings upon repolarization after stimulatory depolarization (Figure 7C), as previously described (Ruppersberg et al., 1991a). Conversely, recovery of MiRP2-Kv3.4 channels was rapid and reopenings could not be resolved despite the presence of similar numbers of channels in the patches (Figure 7C). Neither were reopenings apparent in recordings of native MiRP2-Kv3.4-like single channels in C2C12 muscle cells (Figure 3B) even with recovery pulses lasting 10 s (not shown).

During repetitive stimulation (as in functioning muscles and nerves), a balance between inactivation and recovery from inactivation determines the fraction of voltage-gated ion channels that become unavailable due to cumulative inactivation (Marom, 1998). Cumulative inactivation was assessed here in on-cell patches with alternating 1 s test pulses to +60 mV and 1 s interpulse intervals at −80 mV (Figure 7D). As expected,
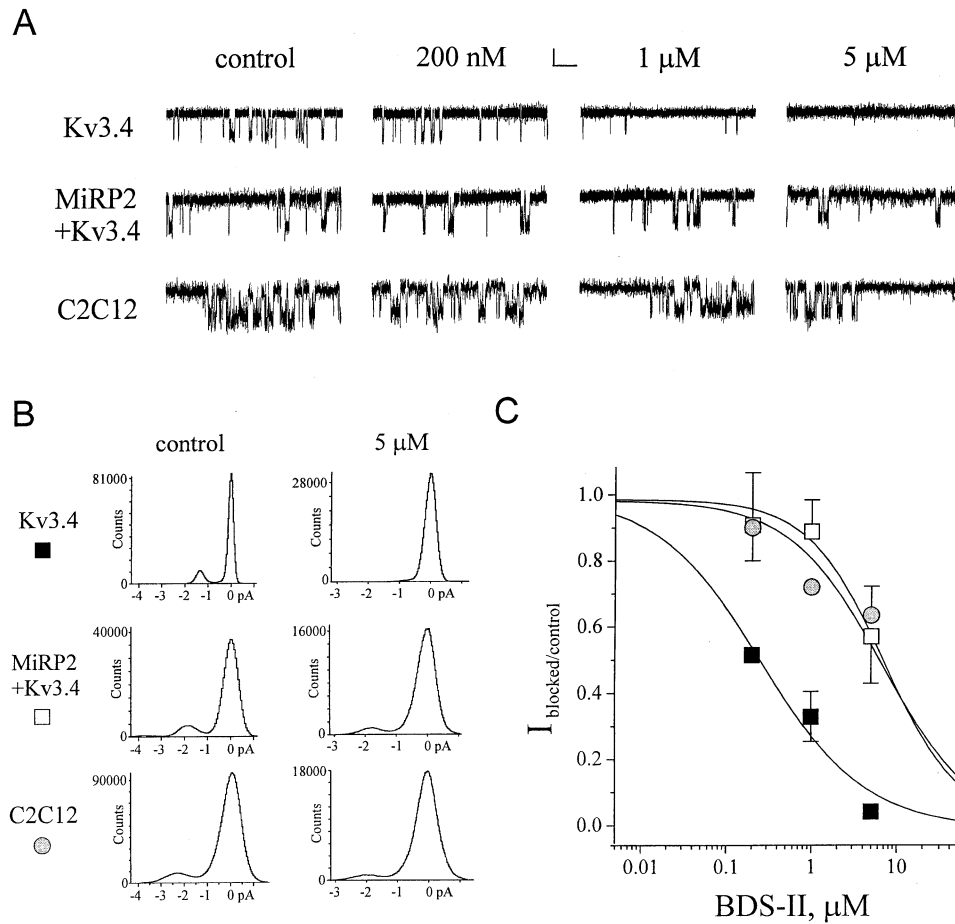
A

B

C

Figure 5. MiRP2-Kv3.4 and Native C2C12 Channels Have Similar Affinities for BDS-II Toxin

Studies of Kv3.4 channels (solid squares) or MiRP2-Kv3.4 channels (open squares) expressed in CHO cells or native C2C12 channels (gray circles) performed in outside-out patches at -40 mV (Protocol 3) with 100 mM KCl solution in bath and pipette; toxin was applied in the bath solution. Low-pass filtered at 500 Hz.

(A) Channel activity in various toxin concentrations as indicated; scale bars 1 pA and 1 s.

(B) Representative all-points histograms from patches at steady state for 5–10 min without toxin (control) or with 5 μM BDS-II and indicative of nP_o.

(C) BDS-II dose-inhibition curves for Kv3.4 channels (solid squares), hMiRP2-Kv3.4 channels (open squares), or native C2C12 channels (gray circles), calculated using all-points histograms as in (B). Each point is the average of 2–3 patches and represents relative nP_o normalized to control nP_o for that patch after toxin washout; error bars are SEM. Curves were fit to the function: $y = [A_1 - A_2 / \{1 + (x/x_0)^p\}] + A_2$ where X is added toxin, x_0 the inhibition constant, and p the Hill coefficient. Kv3.4 channels: $A_1 = 1.00 \pm 0.03$, $A_2 = -0.01 \pm 0.03$, $x_0 = 255 \pm 63$ nM, $p = 0.7 \pm 0.1$; MiRP2-Kv3.4 channels: $A_1 = 0.99 \pm 0.03$, $A_2 = -0.002 \pm 0.04$, $x_0 = 7148 \pm 1785$ nM, $p = 0.97 \pm 0.27$; native C2C12 channels: $A_1 = 0.98 \pm 0.05$, $A_2 = -0.02 \pm 0.05$, $x_0 = 6886 \pm 2706$ nM, $p = 0.79 \pm 0.2$.

more than 50% of Kv3.4 channels were unavailable after just two pulses while MiRP2-Kv3.4 complexes accumulated in the inactive state at least 10-fold more slowly (Figure 7D).

A Missense Mutation in Human MiRP2 Associated with Periodic Paralysis

Based on its expression in human skeletal muscle and function in rodent skeletal muscle cells with Kv3.4, we considered the gene for MiRP2 (*KCNE3*) a candidate for heritable diseases of skeletal muscle that had not been genetically characterized. We therefore screened a panel of 100 patients with inherited or sporadic episodic muscle disorders without mutations in known disease-associated genes (*SCN4A, CACNLA3, CLCN1*) (Ptacek, 1998). Analysis for single-strand conformational poly-

morphism (SSCP) revealed an aberrant conformer in two unrelated individuals (K2706 and K3337) from the affected population with periodic paralysis. This variant was not found in DNA from a control population of 120 unaffected individuals suggesting that it did not represent a polymorphism. DNA sequencing revealed a G340A transition in the *KCNE3* gene predicting an arginine to histidine change at position 83 (R83H-MiRP2). Pedigree analysis of both kindreds revealed three additional family members with periodic paralysis who carried the R83H mutation and two unaffected members who did not (Figure 8A).

The proband in kindred 3337 is male and has had episodes of paralytic weakness since he was 14 years of age. Episodes are characterized by weakness primarily affecting the lower extremities lasting hours to days. The
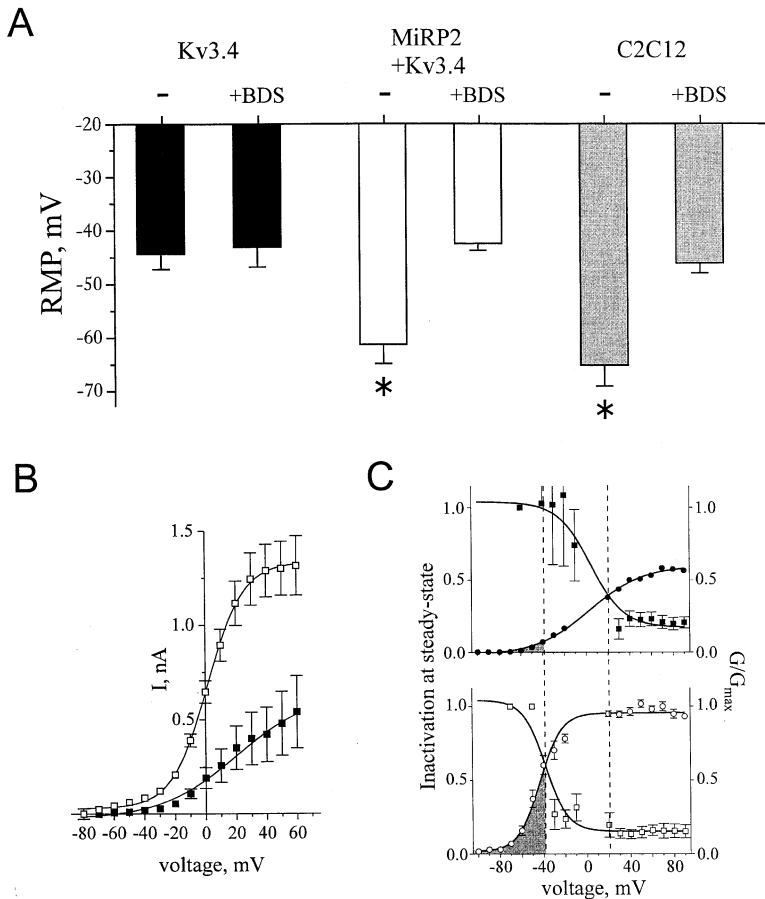
A

B

C

attacks are usually precipitated by strenuous exercise followed by rest or after prolonged sitting. Some attacks occur when he wakes in the morning, but many begin during wakefulness. He has never noticed that high carbohydrate meals precipitate attacks. To the contrary, alcohol intake appears to facilitate recovery from an attack while potassium treatment does not. The patient has not had symptoms of myotonia and none were detected by clinical exam or electromyography (EMG); a lid-lag was detected on a few occasions. The parents were not known to be affected and are deceased. The proband's two brothers and nephew have had similar attacks of weakness (Figure 8A). One brother had onset of symptoms at age 21 but was not examined and is deceased. Muscle biopsy revealed vacuoles and tubular aggregates in both the proband and his other brother, a common finding in all forms of periodic paralysis. With one episode, his serum potassium level was determined to be low (2.1 mmol/l). Provocative testing with insulin and glucose lowered serum potassium and induced weakness on one occasion but not with a second test some years later. Potassium loading failed to induce weakness arguing against the diagnosis of hyperkalemic periodic paralysis (Ptacek, 1998). The proband has had significant reduction in attack frequency and severity when treated with the carbonic anhydrase inhibitor dichlorphenamide, but has developed mild to moderate fixed weakness of the lower extremities. The living brother has very minimal fixed iliopsoas muscle weak-

ness and is not treated. All three of the living affected individuals carry the R83H mutation while an unaffected sister does not (Figure 8A). Taken together, these patients were classified as having hypokalemic periodic paralysis because of the typical age-of-onset, paralytic attacks that most often occur after exercise, a low potassium level during a spontaneous attack, and the ability to precipitate an attack with insulin and glucose on one occasion. Atypical for this diagnosis is that the second provocative test was negative and that attacks more often began during wakefulness.

The proband in kindred 2706 is a boy who presented at 22 months with episodes of weakness. The weakness affects his lower and upper extremities. Most episodes come on during sleep and are brief (1–2 hr) although they occasionally last for days. High carbohydrate meals help to resolve the attacks. At the time of presentation, an EMG did not demonstrate any myotonia and subsequent conduction and EMG studies have not given evidence for neuropathy or myopathy. Serum potassium levels have been measured during attacks and were normal. Provocative testing with potassium has not been performed. Treatment with the carbonic anhydrase inhibitor acetazolamide prevents attacks. The proband's father has muscle cramps in cold water and weakness after exercise although to a less severe degree than his son. Unfortunately, the father has not been available for further evaluation. The age-of-onset, frequent nature of attacks, and improvement with carbohydrate loading are all consis-
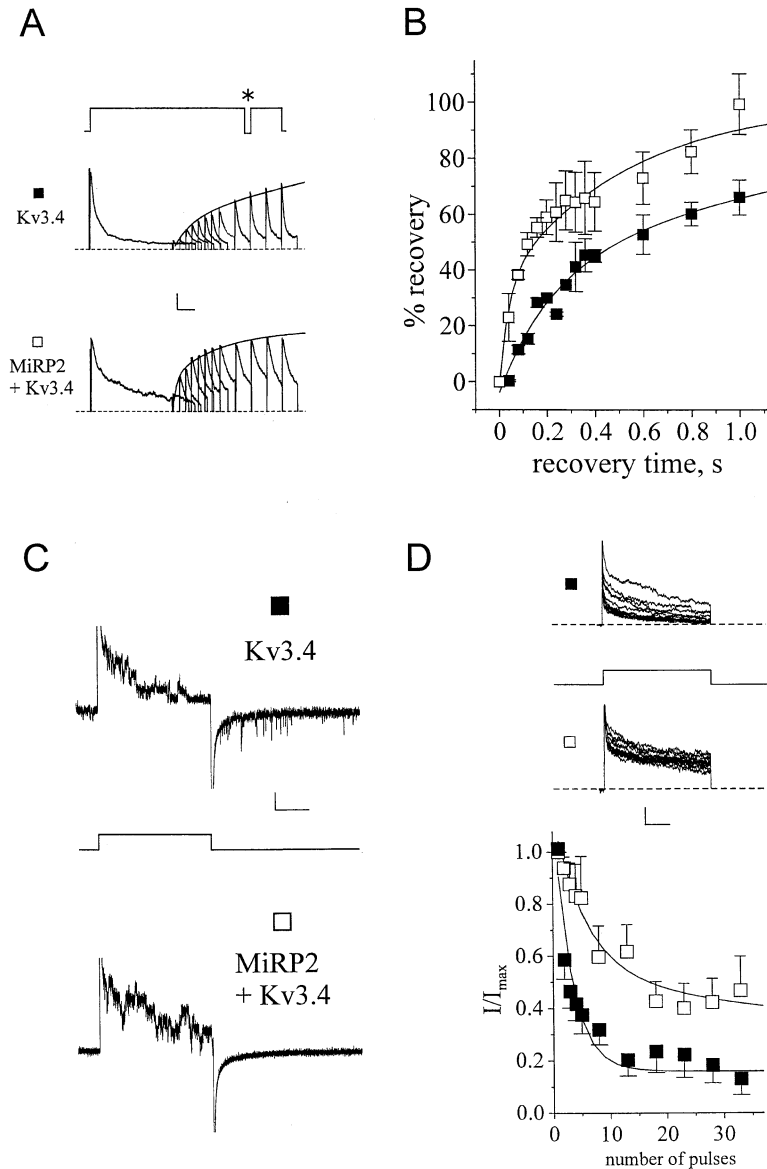
A

B

C

D

Figure 7. MiRP2 Speeds Recovery from Inactivation and Suppresses Cumulative Inactivation

(A) Recovery from inactivation for Kv3.4 channels (solid squares) and MiRP2-Kv3.4 channels (open squares) assessed in whole-cell mode with 4 mM KCl bath solution. (Inset) Protocol 4, asterisk denotes variable recovery phase. For clarity, only the first test pulse is shown and some recovery pulses are omitted. Dashed line is zero current level. Scale bars 300 pA (Kv3.4), 550 pA (MiRP2-Kv3.4), and 100 ms. Double exponential fits indicated.

(B) Mean % recovery of inactivated current-recovery time relationship for whole-cell currents as in (A) (n = 3); error bars indicate SEM. Recovery time course was best fit with a double exponential function of the form: $y = y_o + A_1e^{x/\tau1} + A_2e^{x/\tau2}$. Kv3.4 (solid squares): $\tau_1 = 1.7 \pm 0.7$ s, $A_1 = 0.6 \pm 0.2$; $\tau_2 = 222 \pm 134$ ms, $A_2 = 0.4 \pm 0.2$; MiRP2-Kv3.4 (open squares): $\tau_1 = 520 \pm 30$ ms, $A_1 = 0.7 \pm 0.07$; $\tau_2 = 39 \pm 24$ ms, $A_2 = 0.3 \pm 0.1$.

(C) Representative low current density cell-attached patch traces illustrating extent of reopening during recovery from inactivation (Protocol 5, inset). Traces were recorded with 100 mM KCl in pipette and bath during repetitive pulses and are typical of those observed (n = 12–15 patches). Top panel, Kv3.4, bottom panel, MiRP2-Kv3.4, as indicated.

(D) Cumulative inactivation in cell-attached patches recorded with 100 mM KCl in pipette and bath. Kv3.4, solid squares; MiRP2-Kv3.4, open squares. Top panels: representative traces in train of pulses (Protocol 6, inset). Bottom panel: normalized current with repetitive pulsing as in traces, error bars = SEM (n = 6–8 cells), the first 14 pulses are shown. Cumulative inactivation was fit with a single exponential for Kv3.4 ($y = y_o + Ae^{x/\tau}$; $\tau = 3.0 \pm 0.3$ pulses) while for MiRP2-Kv3.4 it could only be fit with a double exponential function: $y = y_o + A_1e^{x/\tau1} + A_2e^{x/\tau2}$; $\tau_1 = 6 \pm 1$ and $\tau_2 = 75 \pm 15$ pulses, with weights of 0.6 and 0.4, respectively).

tent with hyperkalemic periodic paralysis. However, frequent attacks upon wakening and absence of myotonia are atypical for this diagnosis. Both affected individuals were found to carry the R83H-MiRP2 mutation. The proband's mother is asymptomatic and carries wild-type *KCNE3* genes. His sister was not available for evaluation.

R83H-MiRP2 Reduces MiRP2-Kv3.4 Current Density and Capacity to Set Muscle Cell RMP

To determine if the R83H mutation altered MiRP2-Kv3.4 channel function, its effects on whole-cell peak current amplitudes in CHO cells were first evaluated (Figure 8B); Kv3.4 subunits were expressed with a plasmid control, wild-type MiRP2, or R83H-MIRP2 and studied in 4 mM external potassium. Current density at +50 mV was 27.2 ± 8.3 pA/pF for Kv3.4 channels (n = 8) and 46.0 ± 6.1 pA/pF for wild-type MiRP2-Kv3.4 channels (n = 11); the point mutant reduced current density to 17.1 ± 4.2 pA/pF (n = 10). Further, cells treated with equal amounts

of wild-type and R83H-MiRP2 cDNA (an approximation of the genotype of patients carrying one mutant MiRP2 allele) showed the same low current density (17.8 ± 3.0 pA/pF, n = 8) suggesting that the mutant had a dominant effect (Figure 8B).

To confirm that R83H-MiRP2 altered Kv3.4 function by formation of MiRP2-Kv3.4 channel complexes, sensitivity to BDS-II was evaluated as before (Figure 4). The dose-inhibition relationship for mutant channels gave an inhibition constant of 5.5 ± 1.6 μM, almost the same as that for wild-type MiRP2 and ∼20-fold different than that measured for cloned Kv3.4 channels (Figure 8C). Moreover, there was no evidence that R83H-MiRP2 influenced the function of sodium, calcium, or chloride channels previously associated with periodic paralysis (Ptacek, 1999) as neither wild-type nor mutant MiRP2 subunits altered the attributes of *SCN4A*, *CACNLA3*, or *CLCN1* in experimental cells (not shown).

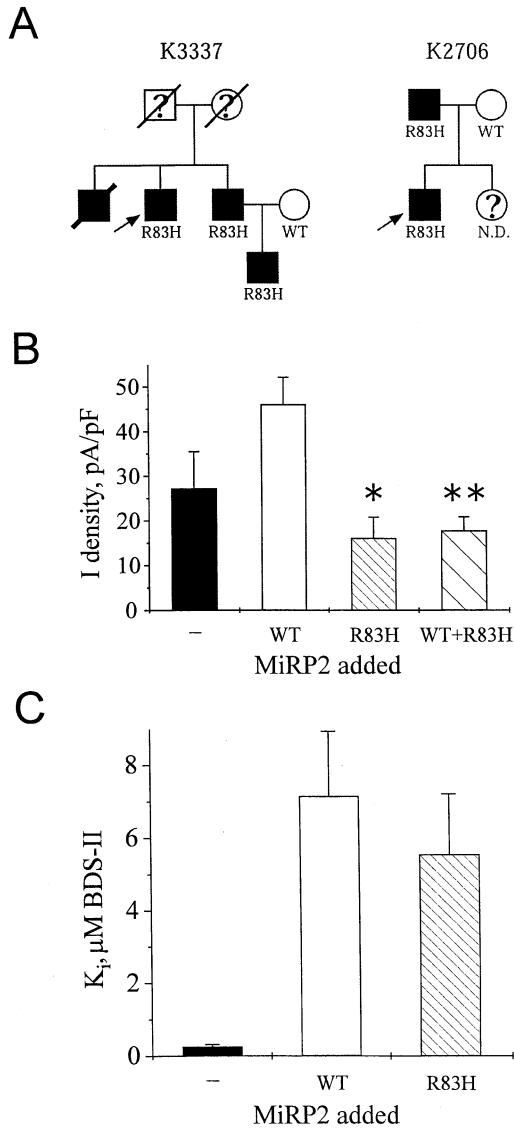R83H-MiRP2 was also found to suppress the capacity

A

K3337   K2706

B

I density, pA/pF

MiRP2 added

C

K_i, μM BDS-II

MiRP2 added

Figure 8. R83H-MiRP2 Is Associated with Familial Periodic Paralysis and Reduced Current Density

(A) Pedigree structure of two kindreds (K2706 and K3337) displaying periodic paralysis. Open symbols represent unaffected individuals, closed symbols patients with periodic paralysis. Genotypes as indicated, N.D. = not determined. Squares indicate males, circles females. Arrow denotes proband. Status unknown (?); deceased (/).
(B) Current density at 50 mV in whole-cell configuration with 4 mM KCl bath solution (Protocol 1) for CHO cells expressing Kv3.4 and (−) a plasmid control, (WT) wild-type MiRP2, (R83H) R83H-MiRP2, or (WT+R83H) equal amounts of wild-type and R83H-MiRP2, as indicated (n = 8–11). Error bars indicate SEM. Single asterisk denotes R83H-MiRP2 current density significantly different than wild-type MiRP2 (P = 0.0014); double asterisk denotes R83H+WT is significantly different than wild-type (P = 0.0025) but not R83H-MiRP2, as assessed by unpaired Student's t test.
(C) Inhibition constant (K_i) for BDS-II blockade of single Kv3.4, MiRP2-Kv3.4, or R83H-MiRP2-Kv3.4 channel currents assessed in outside-out patches at −40 mV (Protocol 3) from dose-inhibition curves as in Figure 5. Error bars are SEM. Dose-response curves were fit as in Figure 5. R83H-MiRP2-Kv3.4 channels: $A_1 = 0.99 \pm 0.04$, $A_2 = -0.02 \pm 0.04$, $X_o = 5540 \pm 1670$ nM, $p = 0.78 \pm 0.2$.
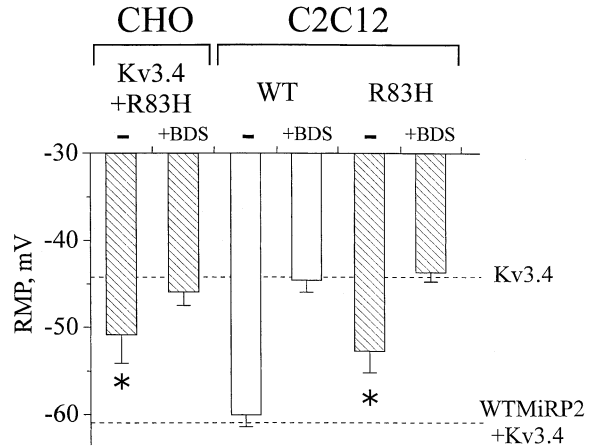

Figure 9. R83H-MiRP2 Has Reduced Capacity to Set RMP with Kv3.4 and Depolarizes C2C12 Muscle Cells

Resting membrane potential (RMP) of CHO cells expressing R83H-MiRP2-Kv3.4 channels or C2C12 cells transfected with wild-type (WT) or R83H-MiRP2 and studied by perforated patch technique as in Figure 6. Cells were bathed in 4 mM KCl solution in the absence (−) (n = 12–14) or presence (+BDS) (n = 6) of 30 μM BDS-II. Error bars are SEM. Dashed lines indicate RMP values determined for CHO cells expressing Kv3.4 or wild-type MiRP2-Kv3.4 channels as reported in Figure 6. Single asterisk denotes RMP values significantly different from wild-type (P = 0.039, CHO cells) or native (P = 0.011, C2C12).

of MiRP2-Kv3.4 complexes to set resting potential in experimental cells. CHO cells expressing R83H-MiRP2-Kv3.4 channels were found to have an RMP of −52 ± 4 mV (n = 9) by the nystatin perforated-patch technique (Figure 9), a value between that determined for cells expressing cloned Kv3.4 channels and those expressing wild-type MiRP2-Kv3.4 channels (−44 mV and −61 mV, respectively, Figure 6A). As before, BDS-II blockade shifted the RMP of cells expressing R83H-MiRP2-Kv3.4 channels to control levels (−46 ± 1 mV, n = 6, Figure 9) suggesting that RMP was mediated by channels containing Kv3.4. Channels with the mutant influenced RMP despite lowered outward current density (while Kv3.4 channels did not) because their steady-state open probability at subthreshold voltages was greater than for channels without MiRP2 (not shown).

R83H-MiRP2 was also found to disrupt the function of native skeletal muscle channels, leading to altered RMP. Thus, when MiRP2 was expressed in C2C12 muscle cells without added Kv3.4, the wild-type subunit produced no significant change in RMP compared to control cells (−65 ± 3 mV, n = 10, Student's t test, P = 0.17) whereas R83H-MiRP2 depolarized the muscle cells to −53 ± 2 mV (the same RMP observed when R83H-MiRP2 and Kv3.4 were overexpressed together in CHO cells, Figure 9). The native channels appeared to contain Kv3.4 as BDS-II caused RMP in both cell types to rise to the level of control cells (−45 ± 1 and −44 ± 1 mV for wild-type and R83H-MiRP2, respectively).

Discussion

The *KCNE* genes encode MinK-related peptides, single transmembrane subunits that are inactive on their own

but essential in native channel complexes (Abbott and Goldstein, 1998). Thus, MinK (from *KCNE1*) and MiRP1 (from *KCNE2*) have been shown to establish key functional attributes in assemblies with KCNQ1 and HERG-type pore-forming subunits: voltage-dependence, gating kinetics, single-channel conductance, ion selectivity, regulation, and pharmacology. Here, we demonstrate that MiRP2 (from *KCNE3*) alters the same attributes as its predecessors, but does so in complexes with Kv3.4, a classical *Shaw*-type subunit. MiRP2 is associated with periodic paralysis and assembles with Kv3.4 in skeletal muscle to form subthreshold, voltage-gated channels that establish RMP. The wide tissue distribution of the MiRPs combined with their capacity to interact with a variety of pore-forming subunits broadens their potential roles in vivo.

MiRP2-Kv3.4 Channel Complexes Recapitulate Potassium Currents in Native Cells

Cloned channel subunits studied in experimental cells often behave differently than the currents attributed to their native counterparts. In some cases, this is due to the absence of channel subunits whether cytoplasmic (Rettig et al., 1994; An et al., 2000) or membrane (Sanguinetti et al., 1996; Abbott et al., 1999). This discrepancy has been particularly notable among the A-type potassium channels (Rizzo and Nonner, 1992; Chabala et al., 1993; Xu et al., 1996). Here, we demonstrate that MiRP2 and Kv3.4 subunits are expressed in skeletal muscle cells (Figure 1); that the biophysical and pharmacological attributes of MiRP2-Kv3.4 channels in CHO cells and native channels in C2C12 cells are similar (Figures 2–5); and, that a disease-associated MiRP2 variant can suppress native channel function in C2C12 muscle cells (Figure 9). These observations argue strongly that MiRP2 and Kv3.4 subunits assemble to form a subthreshold A-type potassium channel in skeletal muscle.

Our findings are also consistent with previous descriptions of cloned Kv3.4 and native A-type channel currents. Rettig and colleagues (Rettig et al., 1992) found the same amplitude and rectification properties for single Kv3.4 channel currents in cell-attached patches as measured here (Figures 2 and 4). More significantly, mild rectification, increased magnitude, and greater steady-state P_o of single MiRP2-Kv3.4 channels (Figures 2 and 4) and native C2C12 channels (Figures 3 and 4) are very like those reported for native voltage-gated channels recorded in vesicles from frog skeletal muscle ($\sim$2 pA at 40 mV, P_o of $\sim$0.05 at –40 mV) (Vazquez, 1988; Camacho et al., 1996) and in normal and denervated murine skeletal muscle fibers ($\sim$2 pA at +50 mV) (Escobar et al., 1993). Further, mean open times for MiRP2-Kv3.4 and native C2C12 cell channels are best fit by a sum of two terms, as previously found for frog skeletal muscle (Vazquez, 1988), although the time constants at -40 mV measured here ($\sim$2.0 ms and 20 ms) are much longer than those observed in frog muscle (0.07 ms and 0.37 ms). Inactivation rates of both cloned and native A-type channels vary widely between cell types and even from cell to cell in the same preparation. This is understood in some cases to result from regulated phosphorylation of N-terminal inactivation "ball" residues (Covarrubias et al., 1994; Antz et al., 1997; Beck et al., 1998). Thus,

the lack of rapidly inactivating potassium currents in mammalian skeletal muscle (Adrian et al., 1970; Beam and Donaldson, 1983; Camacho et al., 1996), despite the robust expression of Kv3.4 in skeletal muscle (Figure 1) (Rettig et al., 1992; Vullhorst et al., 1998), may be explained in part by its assembly with MiRP2, but also appears to reflect regulatory influences. Indeed, we find that inactivation of both Kv3.4 and MiRP2-Kv3.4 channels is more rapid and less variable in *Xenopus* oocytes than in CHO cells (not shown).

A Potential Role in Skeletal Muscle

A role for Kv3.4 subunits in skeletal muscle function has been considered likely because of their high degree of expression in the tissue (Rettig et al., 1992; Weiser et al., 1994; Veh et al., 1995; Vullhorst et al., 1998). Previously, it was suggested that Kv3.4 might modulate inward calcium currents because cloned Kv3.4 channels open in the voltage range where some calcium channels activate, positive to the threshold for sodium channel activation (Schroter et al., 1991). Further, Kv3.4 channels were suspected to play a role in the morphology of action potentials, but not in control of resting potential or the rise to threshold due to their activation at suprathreshold potentials. Finally, the channels were suggested to produce AHPs based on their slow recovery from inactivation (Ruppersberg et al., 1991a). In contrast, our results argue that Kv3.4 channels assemble with MiRP2 in skeletal muscle cells to produce native channels that activate at subthreshold levels, recover rapidly from inactivation, and influence skeletal muscle function. Moreover, expression of wild-type MiRP2 in C2C12 muscle cells had no significant effect while the disease-associated R83H-MiRP2 produced depolarization (Figure 9). This supports a direct role for wild-type MiRP2 subunits in establishing RMP and for the mutant in muscle dysfunction. We conclude that MiRP2-Kv3.4 channels modulate excitability through effects on RMP, rates of rise to threshold, action potential duration, and recovery of sodium channels from inactivation without production of AHPs or cumulative inactivation to limit responsiveness. While MiRP2-Kv3.4 channels appear to be the primary determinant of RMP in undifferentiated C2C12 cells (Figures 6A and 9), their relative contribution in different muscle types (in health and disease) remains to be ascertained. Thus, many vertebrate muscle fibers have a large resting chloride conductance (Bretag, 1987) that is decreased in some forms of inherited and acquired myotonia in association with RMP "instability" (Lehmann-Horn and Jurkat-Rott, 1999).

Other Roles for MiRP2

This study was guided by the prominent expression of MiRP2 and Kv3.4 in skeletal muscle and directed toward understanding recognized discrepancies between cloned channels and native currents in that tissue. Other pore-forming subunits also interact with MiRP2 when studied in experimental cells. Thus, MiRP2 was recently demonstrated to alter the function of both KCNQ1 and HERG when expressed in oocytes and hypothesized to be important to electrolyte balance in the colon (Schroeder et al., 2000). HERG cRNA is not found in adult mammalian skeletal muscle (London et al., 1997; Wymore et al.,

1997) although gene expression is subject to regulation (Arcangeli et al., 1999). Conversely, transcripts for KCNQ1 are present in adult human skeletal muscle, albeit at lower levels than in heart and colon (Yang et al., 1997), suggesting that MiRP2 could influence its function in vivo. KCNQ1 subunits do not appear to be involved in the effects of MiRP2 we describe here; while BDS-II blocks single MiRP2-Kv3.4 channels in both CHO and C2C12 cells and shifts RMP in both cell types, the toxin had no measurable effect on cloned KCNQ1 or MiRP2-KCNQ1 channels (Experimental Procedures). It remains feasible that other pore-forming subunits in skeletal muscle may interact with MiRP2 if their spatial and temporal expression patterns overlap. As we did not detect MiRP2 in human colonic poly(A)$^+$ mRNA (Figure 1A), and Schroeder and colleagues (2000) did not demonstrate the presence of MiRP2 peptide or MiRP2-KCNQ1-like currents in colon cells, the contention that MiRP2 functions in that tissue requires further support.

A MiRP2 Mutation Associated with Periodic Paralysis

Association of a potassium channel subunit (R83H-MiRP2) with periodic paralysis is novel but consistent with current thinking on the etiology of these disorders. In each case, paralysis is associated with an abnormally positive skeletal muscle resting membrane, disrupted sodium channel inactivation, and altered excitability. With mutant MiRP2-Kv3.4 channels, this appears to result from decreased outward potassium flux producing a more positive RMP and reduced repolarization capacity. The functional effects we observe and correlation of genotype and phenotype in our patients support a causative role for R83H-MiRP2 in periodic paralysis. To reinforce this conclusion and explore the basis for symptomatic differences between individuals, additional patients will be sought.

Familial hyperkalemic periodic paralysis has been associated with mutants of the SCN4A voltage-gated sodium channel (encoded on chromosome 17q) (Ptacek et al., 1991) that are too active either because they open at abnormally negative potentials (Cummins et al., 1993) or inactivate too slowly (Cannon and Strittmatter, 1993; Cummins and Sigworth, 1996). Both changes increase inward sodium flux leading to membrane depolarization and impaired repolarization. Similarly, familial hypokalemic periodic paralysis has been associated with inexcitability and a skeletal muscle RMP more positive than normal (Lehmann-Horn and Jurkat-Rott, 1999) due to mutations in the gene for the L-type calcium channel encoded on chromosome 1q31-q32 (Fontaine et al., 1994; Ptacek et al., 1994) and the SCN4A sodium channel (Bulman et al., 1999; Jurkat-Rott et al., 2000). So, too, barium toxicity, a rare but well-documented cause of acute periodic paralysis, reduces potassium efflux from muscle cells (due in part to potassium channel blockade) leading to membrane depolarization and muscle cells that are inexcitable (Layzer, 1982). Even chloride channel mutations can cause transient weakness in a related muscle disorder (Ptacek, 1998). The previous lack of recognition of potassium channel mutations in periodic paralysis has been conspicuous based on our knowledge of membrane physiology.

The familial periodic paralyses are rare disorders classified by their clinical features such as age of onset, time of day, frequency of attacks, and measures that can provoke attacks (e.g., response to altered serum potassium level or other dietary factors). Because the disorders are clinically and genetically heterogeneous, the overlapping signs, symptoms, and responses to therapy have complicated diagnosis. Identification of the underlying genetic basis has led to a new classification system based on the molecular defects that have been found (Ptacek, 1998). This new scheme has aided clinicians in diagnosis of the periodic paralyses and allowed implementation of a therapeutic trial of dichlorpenamide with patients enrolled based on characterization of their specific mutations. While such carbonic anhydrase inhibitors are anecdotally beneficial in many patients, one study has shown benefit in a blinded and controlled fashion (Tawil et al., 2000). This was likely due, in part, to enrollment of a study cohort that was relatively homogeneous at a molecular level. The association of KCNE3 mutations with clinical presentations that are not characteristic of either classical hyper- or hypokalemic periodic paralysis emphasizes the clinical complexity of these disorders and the need for diagnosis based on genotype. Increasingly, such classification should improve our ability to diagnose and treat these patients.

Experimental Procedures

Study Subjects and Mutational Analysis

The GenBank accession numbers for human and mouse MiRP2 (KCNE3) are AF076531 and AF076532, respectively. Clinical studies and sampling of family members were conducted after subjects signed a consent form approved by the Institutional Review Board of the University of Utah Health Sciences Medical Center. Genomic DNA was isolated from peripheral blood leukocytes, amplified using PCR, and single-strand conformational polymorphism (SSCP) analysis performed (Orita et al., 1989). Oligonucleotide primer pairs used to amplify KCNE3 for SSCP were section I (nucleotides 48–267 of accession number AF076531), forward primer: 5′-GTTTGAGCTT CTACCGAG-3′; reverse primer: 5′-TGTAGGAGTTGTCATCAC-3′; section II (corresponding to nucleotides 212–482), forward primer: 5′-CAACCAGACTGAAGAGAG-3′; reverse primer: 5′-CAGTCCAC AGCAGAGTTC-3′. Amplification reactions were carried out and samples analyzed as before (Ptacek et al., 1992). Abnormal conformers were eluted and re-amplified for sequencing by dye termination chemistry. The presence of the R83H-MiRP2 mutation was confirmed independently by PCR amplification of patient genomic DNA and sequencing (Ptacek et al., 1992).

Heterologous Expression

The mutation was produced in wild-type human KCNE3 in pGA1 as before (Abbott et al., 1999). The gene for rat Kv3.4 (Accession number Q63734) was generously provided by B. Fakler (Tubingen). For studies in oocytes, cRNA was transcribed for MiRP2 and Kv3.4 genes in pGA1 as before (Abbott et al., 1999). Transient transfection of CHO, COS, and C2C12 cells was achieved with lipid-based reagents and a vector carrying the gene for green fluorescent protein (GFP). MIRP2, Kv3.4, and GFP were expressed in pCl-neo-based vectors (Promega).

Purification of Recombinant MIRP2 and Antibody Production

The coding region of mouse KCNE3 encoding MIRP2 was subcloned into the bacterial expression vector, pGEX6P-1 (Amersham Pharmacia Biotech, Piscataway, NJ) and MIRP2 purified by solubilization with 1% (w/w) sarkosyl followed by 1.3% Triton X-100 and cleavage from its GST fusion product with Prescission protease (Amersham Pharmacia). MiRP2 was subjected to SDS-PAGE, visualized with

coomasie blue, excised from the gel, and injected into rabbits (Pocono Rabbit Farm, Canadensis, PA). Immunoglobulin was affinity purified with Protein-A sepharose beads (Amersham Pharmacia) and specific antibody purified with a MiRP2-loaded PVDF membrane (Immobilon-P, Millipore Corporation, Bedford, MA). Affinity-purified antibody was used in all experiments.

Protein Biochemistry
Crude membrane fractions were prepared from freshly collected rat sartorius skeletal muscle using a tissue disruptor. Complete Protease Inhibitor Cocktail (Roche, Indianapolis, IN) was included in all buffer solutions used for protein preparation. Muscle homogenates (20 g) in 30 ml of 320 mM sucrose, 5 mM HEPES (pH 7.5) were centrifuged (3K $\times$ g) and filtered through Miracloth (Calbiochem-Novabiochem Corporation, San Diego, CA). After adding KCl to 0.5 M, the homogenate was incubated on ice for 10 min and centrifuged at 48K $\times$ g for 40 min and the pellet washed twice in 150 mM NaCl, 10 mM HEPES (pH 7.5). The resulting pellet was solubilized in SDS-PAGE loading buffer for Western blot analysis (100 μg/lane).

CHO cells were harvested 24 hr after transfection, solubilized with PBS containing 1% CHAPS, 1% Triton X-100, 1% NP-40, 0.5% SDS before centrifugation at 50K $\times$ g for 20 min. The supernatant was used directly for Western blot analysis (100 μg/lane) or denatured by boiling in 0.5% SDS prior to treatment with endoglycosidase F (Roche, Indianapolis, IN) overnight at 37°C (1 U per 100 μg protein) in 0.5 M Tris (pH 8), 0.25% Triton X-100. C2C12 cells were harvested by centrifugation 2–5 days after replating using PBS containing 10 mM EDTA and then resuspended in 150 mM NaCl, 10 mM HEPES (pH 7.5), 2% Triton X-100, and 0.25% SDS. Western blot analysis was performed with 100 μg protein per lane. Endoglycosidase F treatment of C2C12 cell lysates was followed by precipitation with 10% TCA.

Coimmunoprecipitation of MiRP2 and Kv3.4 in COS-7 cells was similar to previous methods (Abbott et al., 1999) except that the complex was isolated with a commercial polyclonal anti-Kv3.4 antibody (Alomone Labs, Jerusalem, Israel) using 10 μg antibody with 1.5 mg total protein.

Western and Northern Blot Analyses
Western blot analyses were performed as previously (Abbott et al., 1999) except for evaluation of MIRP2 where SDS was omitted from the transfer buffer and the transfer was conducted at 75 volts for 1 hr to enhance retention and detection of small proteins. Both MIRP2 and Kv3.4 antibodies were used at a dilution of 1:200 and anti-HA at 1:1000. Proteins were detected using either HRP-conjugated anti-rabbit or anti-mouse secondary antibodies (Sigma-Aldrich) and ECL reagents (Pierce, Rockford, IL).

Northern blots were performed with ^{32}P[ATP]-labeled probes (Amersham Pharmacia), first with the 1060 bp fragment of human *KCNE3* contained on EST AA132718, then with β-actin cDNA; the specific labeling was identical using a 133 bp portion of the *KCNE3* 3′UTR (42–174), not shown. The membranes were purchased (Clontech) and contained 2 μg poly(A)$^{+}$ mRNA purified from 16 human tissues. While a single strong message was observed in skeletal muscle (and weak bands in heart and brain transcripts after extended exposure), no message was visualized in ovary, testis, prostate, thymus, spleen, or the other eight tissues shown in Figure 1A.

Surface Immunostaining of C2C12 Muscle Cells
48 hr after plating onto cover slips, C2C12 cells were incubated with primary antibody for 1 hr, washed, fixed with 4% paraformaldehyde, and incubated with either CY3-conjugated goat anti-rabbit secondary antibody (for Kv3.4) or Oregon Green-conjugated goat anti-rabbit secondary antibody (MiRP2 and negative control) for immunofluorescence microscopy.

Oocyte Studies
Coexpression of MiRP2 with Kv1.4, Kv4.1, and Kv3.4 subunits was initially studied in *Xenopus* oocytes using two-electrode voltage clamp and 4 mM potassium solutions, as previously described (Abbott et al., 1999). While Kv1.4 and Kv4.1 currents showed no apparent differences when coexpressed with MiRP2, Kv3.4 currents showed altered resting membrane potential, voltage-dependent

conductance, and BDS-II sensitivity (not shown). MiRP2 is now under study in oocytes with KCNQ1, which produces a "leak" channel phenotype (Schroeder et al., 2000); 30 μM BDS-II had no apparent effect on KCNQ1 or MiRP2-KCNQ1 currents in oocytes (not shown).

Electrophysiology with CHO and C2C12 Cells
For detailed characterization, Kv3.4 and MiRP2-Kv3.4 channels were assessed using Chinese hamster ovary (CHO) cells by whole cell or patch clamp 1–3 days after transfection. C2C12 murine skeletal muscle cells are derived from 129 ReJ mice (Yaffe and Saxel, 1977) and were allowed to grow to a semi-confluent state (2–5 days), split, replated, and allowed to grow 2–3 additional days prior to recording. CHO and C2C12 cell recording was with an Axopatch 200A Amplifier (Axon Instruments, Foster City, CA), an IBM computer, and CLAMPEX software (Axon Instruments). Data analysis was performed using CLAMPFIT, FETCHAN, PSTAT (Axon Instruments), and TAC software (Instrutech, Great Neck, NY). All experiments were performed at room temperature.

Patches from C2C12 cells most frequently contained two or three MiRP2-Kv3.4-like channels (<10% single-channel patches) and are reported as nP$_o$ and "apparent first latency"; expression levels were varied to achieve single-channel patches for CHO cell recordings.

Protocols
Holding voltage was −80 mV unless otherwise stated. (1) Peak and steady-state current; 3 s pulse from −100 to 90 mV in 10 mV steps with a 5 s interpulse interval. (2) Single voltage; repetitive 3 s pulses to a single voltage as indicated with a 5 s interpulse interval. (3) Steady-state; holding at −40 mV for 5–20 min with no interpulse interval. (4) Inactivation recovery; 3 s depolarizing pulse to 30 mV followed by −90 mV recovery pulses of increasing duration in 40 ms steps; interpulse interval 5 s. (5) Recovery (reopening); repetitive 1.5 s pulses to 60 mV with a 5 s interpulse interval. (6) Cumulative inactivation; repetitive 1 s pulses to 60 mV with 1 s total interpulse interval.

Ionic Conditions
Pipette solution for CHO cells in on-cell mode was (in mM): 100 KCl, 0.7 MgCl$_2$, 1 CaCl$_2$, 10 HEPES (pH 7.4). CHO cell bath solution was as in the pipette or 4 mM KCl, 96 mM NaCl instead of 100 mM KCl for whole-cell recording. Cell-attached recordings with C2C12 cells were performed with a pipette solution (in mM): 100 KCl, 0.7 MgCl, 1 EGTA, 10 HEPES (pH 7.4) and no added calcium and bath solutions as above. For all outside-out recordings pipette and bath solution was (in mM): 100 KCl, 0.7 MgCl, 1 EGTA, 10 HEPES (pH 7.4).

BDS-II Studies
Outside-out patches were held at −40 mV and toxin applied externally via the bath solution containing 0.1% BSA. To ensure rundown did not introduce artifacts, open probability was assessed after toxin washout and the patch was discarded if channel activity did not return to within 10% of baseline (<20% of patches). BDS-II applied in the pipette in on-cell patches (where rundown is not seen) gave the same apparent affinity for both Kv3.4 and MiRP2-Kv3.4 channels (n = 3, not shown).

Perforated Patch Technique
This was performed with nystatin (Sigma) at a final concentration of 150 μg/ml in the pipette solution. After filling the tip with normal pipette solution, nystatin solution was used to back-fill. After seal formation, patches were held at −80 mV for 30 s, then resting membrane potential was measured in current-clamp configuration after attainment of whole-cell configuration as assessed by resistance testing.

References

Abbott, G.W., and Goldstein, S.A.N. (1998). A superfamily of small potassium channel subunits: form and function of the MinK-related peptides (MiRPs). Quarterly Reviews Biophysics *31*, 357–398.

Abbott, G.W., Sesti, F., Splawski, I., Buck, M., Lehmann, M.H., Timothy, K.W., Keating, M.T., and Goldstein, S.A.N. (1999). MiRP1 forms IKr potassium channels with HERG and is associated with cardiac arrhythmia. Cell *97*, 175–187.

Adrian, R.H., Chandler, W.K., and Hodgkin, A.L. (1970). Voltage-clamp experiments in striated muscle fibres. J. Physiol. (Lond.) *208*, 607–644.

An, W.F., Bowlby, M.R., Bett, M., Cao, J., Ling, H.P., Mendoza, G., Hinson, J.W., Mattsson, K.I., Strassle, B.W., Trimmer, J.S., and Rhodes, K.J. (2000). Modulation of A-type potassium channels by a family of calcium sensors. Nature *403*, 553–556.

Antz, C., Geyer, M., Fakler, B., Schott, M.K., Guy, H.R., Frank, R., Ruppersberg, J.P., and Kalbitzer, H.R. (1997). NMR structure of inactivation gates from mammalian voltage-dependent potassium channels. Nature *385*, 272–275.

Arcangeli, A., Rosati, B., Crociani, O., Cherubini, A., Fontana, L., Passani, B., Wanke, E., and Olivotto, M. (1999). Modulation of HERG current and herg gene expression during retinoic acid treatment of human neuroblastoma cells: potentiating effects of BDNF. J. Neurobiol. *40*, 214–225.

Barhanin, J., Lesage, F., Guillemare, E., Fink, M., Lazdunski, M., and Romey, G. (1996). K(V)LQT1 and IsK (minK) proteins associate to form the I(Ks) cardiac potassium current. Nature *384*, 78–80.

Beam, K.G., and Donaldson, P.L. (1983). A quantitative study of potassium channel kinetics in rat skeletal muscle from 1 to 30 degrees C. J. Gen. Physiol. *81*, 485–512.

Beck, E.J., Sorenson, R.G., Slater, S.J., and Covarrubias, M. (1998). Interactions between multiple phophorylation sites in the inactivation particle of a K+ channel. J. Gen. Physiol. *112*, 71–84.

Bretag, A.H. (1987). Muscle chloride channels. Physiol. Rev. *67*, 618–724.

Bulman, D.E., Scoggan, K.A., van Oene, M.D., Nicolle, M.W., Hahn, A.F., Tollar, L.L., and Ebers, G.C. (1999). A novel sodium channel mutation in a family with hypokalemic periodic paralysis. Neurology *53*, 1932–1936.

Camacho, J., Delay, M.J., Vazquez, M., Arguello, C., and Sanchez, J.A. (1996). Transient outward K+ channels in vesicles derived from frog skeletal muscle plasma membranes. Biophys. J. *71*, 171–181.

Cannon, S.C., and Strittmatter, S.M. (1993). Functional expression of sodium channel mutations identified in families with periodic paralysis. Neuron *10*, 317–326.

Chabala, L.D., Bakry, N., and Covarrubias, M. (1993). Low molecular weight poly (A)+ mRNA species encode factors that modulate gating of a non-*Shaker* A-type K+ channel. J. Gen. Physiol. *102*, 713–728.

Covarrubias, M., Wei, A., and Salkoff, L. (1994). Elimination of rapid potassium channel inactivation by phosphorylation of the inactivation gate. Neuron *13*, 1403–1412.

Cummins, T.R., and Sigworth, F.J. (1996). Impaired slow inactivation in mutant sodium channels. Biophys. J. *71*, 227–236.

Cummins, T.R., Zhou, J., Sigworth, F.J., Ukomadu, C., Stephan, M., Ptacek, L.J., and Agnew, W.S. (1993). Functional consequences of a Na+ channel mutation causing hyperkalemic periodic paralysis. Neuron *10*, 667–678.

Diochot, S., Schweitz, H., Beress, L., and Lazdunski, M. (1998). Sea anemone peptides with a specific blocking activity against the fast inactivating potassium channel Kv3.4. J. Biol. Chem. *273*, 6744–6749.

Escobar, A.L.M., Schinder, A.F., Biali, F.I., Siri, L.C.N., and Uchitel, O.D. (1993). Potassium channels from normal and denervated mouse skeletal muscle fibres. Muscle and Nerve *16*, 579–586.

Fontaine, B., Vale-Santos, J., Jurkat-Rott, K., Reboul, J., Plassart, E., Rime, C.S., Elbaz, A., Heine, R., Guimaraes, J., Weissenbach, J., et al. (1994). Mapping of the hypokalaemic periodic paralysis (HypoPP) locus to chromosome 1q31–32 in three European families. Nat. Genet. *6*, 267–272.

Jurkat-Rott, K., Mitrovic, N., Hang, C., Kouzmekine, A., Iaizzo, P., Herzog, J., Lerche, H., Nicole, S., Vale-Santos, J., Chauveau, D., et al. (2000). Voltage-sensor sodium channel mutations cause hypokalemic periodic paralysis type 2 by enhanced inactivation and reduced current. Proc. Natl. Acad. Sci. USA *97*, 9549–9554.

Layzer, R.B. (1982). Periodic paralysis and the sodium-potassium pump. Ann. Neurol. *11*, 547–552.

Lehmann-Horn, F., and Jurkat-Rott, K. (1999). Voltage-gated ion channels and hereditary disease. Physiol. Rev. *79*, 1317–1372.

Lesage, F., Attali, B., Lazdunski, M., and Barhanin, J. (1992). Developmental expression of voltage-sensitive K+ channels in mouse skeletal muscle and C2C12 cells. FEBS Lett. *310*, 162–166.

London, B., Trudeau, M.C., Newton, K.P., Beyer, A.K., Copeland, N.G., Gilbert, D.J., Jenkins, N.A., Satler, C.A., and Robertson, G.A. (1997). Two isoforms of the mouse ether-a-go-go-related gene co-assemble to form channels with properties similar to the rapidly activating component of the cardiac delayed rectifier K+ current. Circ. Res. *81*, 870–878.

Marom, S. (1998). Slow changes in the availability of voltage-gated ion channels: effects on the dynamics of excitable membranes. J. Membr. Biol. *161*, 105–113.

Orita, M., Iwahana, H., Kanazawa, H., Hayashi, K., and Sekiya, T. (1989). Detection of polymorphisms of human DNA by gel electrophoresis as single-strand conformation polymorphisms. Proc. Natl. Acad. Sci. USA. *86*, 2766–2770.

Piccini, M., Vitelli, F., Seri, M., Galietta, L.J., Moran, O., Bulfone, A., Banfi, S., Pober, B., and Renieri, A. (1999). KCNE1-like gene is deleted in AMME contiguous gene syndrome: identification and characterization of the human and mouse homologs. Genomics *60*, 251–257.

Ptacek, L.J. (1998). The familial periodic paralyses and nondystrophic myotonias. Am. J. Med. *105*, 58–70.

Ptacek, L.J. (1999). Ion channel diseases: episodic disorders of the nervous system. Semin. Neurol. *19*, 363–369.

Ptacek, L.J., George, A.L., Jr., Griggs, R.C., Tawil, R., Kallen, R.G., Barchi, R.L., Robertson, M., and Leppert, M.F. (1991). Identification of a mutation in the gene causing hyperkalemic periodic paralysis. Cell *67*, 1021–1027.

Ptacek, L.J., George, A.L., Jr., Barchi, R.L., Griggs, R.C., Riggs, J.E., Robertson, M., and Leppert, M.F. (1992). Mutations in an S4 segment of the adult skeletal muscle sodium channel cause paramyotonia congenita. Neuron *8*, 891–897.

Ptacek, L.J., Tawil, R., Griggs, R.C., Engel, A.G., Layzer, R.B., Kwiecinski, H., McManis, P.G., Santiago, L., Moore, M., Fouad, G., et al. (1994). Dihydropyridine receptor mutations cause hypokalemic periodic paralysis. Cell *77*, 863–868.

Rettig, J., Wunder, F., Stocker, M., Lichtinghagen, R., Mastiaux, F., Beckh, S., Kues, W., Pedarzani, P., Schroter, K.H., and Ruppersberg, J.P. (1992). Characterization of a Shaw-related potassium channel family in rat brain. EMBO J. *11*, 2473–2486.

Rettig, J., Heinemann, S.H., Wunder, F., Lorra, C., Parcej, D.N., Dolly, J.O., and Pongs, O. (1994). Inactivation properties of voltage-gated K+ channels altered by presence of beta-subunit. Nature *369*, 289–294.

Rizzo, M.A., and Nonner, W. (1992). Transient K current in the somatic membrane of cultured central neurons of embryonic rat. J. Neurophys. *68*, 1708–1719.

Rudy, B., Hoger, J.H., Lester, H.A., and Davidson, N. (1988). At least two mRNA species contribute to the properties of rat brain A-type potassium channels expressed in *Xenopus* oocytes. Neuron *1*, 649–658.

Ruppersberg, J.P., Frank, R., Pongs, O., and Stocker, M. (1991a). Cloned neuronal IK(A) channels reopen during recovery from inactivation. Nature *353*, 657–660.

Ruppersberg, J.P., Stocker, M., Pongs, O., Heinemann, S.H., Frank, R., and Koenen, M. (1991b). Regulation of fast inactivation of cloned mammalian IK(A) channels by cysteine oxidation. Nature *352*, 711–714.

Sanguinetti, M.C., Curran, M.E., Zou, A., Shen, J., Spector, P.S., Atkinson, D.L., and Keating, M.T. (1996). Coassembly Of K(V)Lqt1 and Mink (Isk) proteins to form cardiac I-Ks potassium channel. Nature *384*, 80–83.

Schroeder, B.C., Waldegger, S., Fehr, S., Bleich, M., Warth, R., Greger, R., and Jentsch, T.J. (2000). A constitutively open potassium channel formed by KCNQ1 and KCNE3. Nature *403*, 196–199.

Schroter, K.H., Ruppersberg, J.P., Wunder, F., Rettig, J., Stocker, M., and Pongs, O. (1991). Cloning and functional expression of a TEA-sensitive A-type potassium channel from rat brain. FEBS Lett. *278*, 211–216.

Sesti, F., and Goldstein, S.A.N. (1998). Single-channel characteristics of wildtype IKs channels and channels formed with two minK mutants that cause long QT syndrome. J. Gen. Physiol. *112*, 651–664.

Sesti, F., Abbott, G.W., Wei, J., Murray, K.T., Saksena, S., Schwartz, P.J., Priori, S.G., Roden, D.M., George, A.L.J., and Goldstein, S.A.N. (2000). A common polymorphism associated with antibiotic-induced cardiac arrhythmia. Proc. Natl. Acad. Sci. USA *97*, 10613–10618.

Splawski, I., Tristani-Firouzi, M., Lehmann, M.H., Sanguinetti, M.C., and Keating, M.T. (1997). Mutations in the hminK gene cause long QT syndrome and suppress IKs function. Nat. Genet. *17*, 338–340.

Takumi, T., Ohkubo, H., and Nakanishi, S. (1988). Cloning of a membrane protein that induces a slow voltage-gated potassium current. Science *242*, 1042–1045.

Tawil, R., McDermott, M.P., Brown, R., Jr., Shapiro, B.C., Ptacek, L.J., McManis, P.G., Dalakas, M.C., Spector, S.A., Mendell, J.R., Hahn, A.F., and Griggs, R.C. (2000). Randomized trials of dichlorphenamide in the periodic paralyses. Working Group on Periodic Paralysis. Ann. Neurol. *47*, 46–53.

Vazquez, M. (1988). Single-channel analysis of fast transient outward K+ currents in frog skeletal muscle. Eur. J. Physiol. *436*, 95–103.

Veh, R.W., Lichtinghagen, R., Sewing, S., Wunder, F., Grumbach, I.M., and Pongs, O. (1995). Immunohistochemical localization of the Kv1 channel subunits: contrasting subcellular locations and neuron-specific co-localizations in rat brain. Eur. J. Neurosci. *7*, 2189–2205.

Vullhorst, D., Klocke, R., Bartsch, J.W., and Jockusch, H. (1998). Expression of the potassium channel Kv3.4 in mouse skeletal muscle parallels fiber type maturation and depends on excitation pattern. FEBS Lett. *421*, 259–262.

Weiser, M., V.-S. de Miera, E., Kentros, C., Moreno, H., Franzen, L., Hillman, D., Baker, H., and Rudy, B. (1994). Differential expression of *Shaw*-related K+ channels in the rat central nervous system. J. Neurosci. *14*, 949–972.

Wymore, R.S., Gintant, G.A., Wymore, R.T., Dixon, J.E., McKinnon, D., and Cohen, I.S. (1997). Tissue and species distribution of mRNA for the IKr-like K+ channel, erg. Circ. Res. *80*, 261–268.

Xu, H., Dixon, J.E., Barry, D.M., Trimmer, J.S., Merlie, J.P., McKinnon, D., and Nerbonne, J.M. (1996). Developmental analysis reveals mismatches in the expression of K+ channel alpha subunits and voltage-gated K+ channel currents in rat ventricular myocytes. J. Gen. Physiol. *108*, 405–419.

Yaffe, D., and Saxel, O. (1977). Serial passaging and differentiation of myogenic cells isolated from dystrophic mouse muscle. Nature *270*, 725–727.

Yang, W.P., Levesque, P.C., Little, W.A., Conder, M.L., Shalaby, F.Y., and Blanar, M.A. (1997). KvLQT1, a voltage-gated potassium channel responsible for human cardiac arrhythmias. Proc. Natl. Acad. Sci. USA. *94*, 4017–4021.